Pure Appl. Chem., Vol. 72, Nos. 1–2, pp. 245–255, 2000.

Effect of atmospheric oxidation on the electronic and photoluminescence properties of silicon nanocrystals*

I. N. Germanenko[1], M. Dongol[1,‡], Y. B. Pithawalla[1], M. Samy El-Shall[1,†], and J. A. Carlisle[2]

[1]Department of Chemistry and [2]Department of Physics, Virginia Commonwealth University, Richmond, Virginia 23284 USA

Abstract: Web-like aggregates of coalesced Si nanocrystals produced by a laser vaporization-controlled condensation technique show luminescence properties that are similar to those of porous Si. The results are consistent with a quantum confinement mechanism as the source of the red photoluminescence (PL) in this system. The oxidized Si nanoparticles do not exhibit the red PL that is characteristic of the surface-oxidized Si nanocrystals. The nanoparticles are allowed to oxidize slowly, and the PL is measured as a function of the exposure time in air. A significant blue shift in the red PL peak is observed as a result of the slow oxidation process. The dependence of quantum size effects on the bonding structure is established by correlating the PL data with the photon-yield electronic structure measurements made at the Advanced Light Source. The results indicate that as the nanoparticles oxidize, the radius of the crystalline core decreases in size, which gives rise to a larger bandgap and consequently to the observed blue-shift in the PL band. The correlation between the PL, SXF, and NEXAFS results provides further support for the quantum confinement mechanism as the origin of the visible PL in Si nanocrystals.

INTRODUCTION

The remarkable discovery of photoluminescence (PL) from porous Si has led to great interest in the synthesis and properties of Si nanocrystals because they are believed to be the luminescent centers in porous Si [1–8]. Research in this area is motivated by the possibility of designing Si-based nanostructured materials that possess novel electronic and optical properties that can be used in new devices for optical communication [8].

In a recent study, we investigated the physical, optical, and PL properties of Si nanocrystals prepared by a laser vaporization-controlled condensation (LVCC) technique [9–11]. The web-like aggregates of coalesced Si nanocrystals, passivated by a SiO_x barrier layer, exhibit red PL upon excitation with visible or UV light. This emission is characterized by a multiexponential decay having a long component that increases in lifetime (50–100 μs at 300 K) and intensity with emission wavelength (630–740 nm). Although many different mechanisms have been proposed to explain the visible PL from porous Si and Si nanocrystals [1–16], most of the PL properties of Si nanocrystals can be explained by the quantum confinement mechanism [6–11]. According to an extended version of this mechanism, the larger bandgap in Si nanocrystals is attributed to quantum-confined Si structures where

Pure Appl. Chem.* **72, 1–331 (2000). An issue of reviews and research papers based on lectures presented at the 1st IUPAC Workshop on Advanced Materials (WAM1), Hong Kong, July 1999, on the theme of nanostructured systems.
†Corresponding author
‡Permanent address: Physics Department, Faculty of Science, South Valley University, Qena, Egypt

recombination of electrons and holes occurs in a surface state [17, 18]. The long annealing time in ambient air required before emission can be observed, can be explained by the formation of an efficient surface oxide layer that enhances the radiative recombination in the crystallites by removing competitive nonradiative relaxation at the surface. This long passivation time may suggest that slow continuous oxidation of the Si core takes place in ambient air and this process may result in a gradual decrease of the core size. Accordingly, the red PL is observed only when the size of the Si core becomes comparable to the quantum confinement regime.

In this paper, we provide evidence for shrinking the size of the silicon core in surface-oxidized Si nanocrystals as a result of further oxidation in air. We also correlate the changes in the PL of the Si nanocrystals with electronic structure measurements made using photon-in, photon-out techniques at the Advanced Light Source (ALS) [19]. Photon-yield-based techniques such as soft-X-ray fluorescence spectroscopy (SXF) and photon-yield near-edge X-ray absorption fine structure (PY-NEXAFS) have emerged as powerful tools that can characterize materials intractable to other traditional spectroscopy. SXF and PY-NEXAFS are intrinsically bulk sensitive, element-selective probes of occupied and unoccupied electronic structure, respectively [19]. They also have the advantage of being insensitive to charging effects and surface oxidation.

The organization of the paper is as follows. First, we provide a brief description of the LVCC method to synthesize the Si nanocrystals. In the results and discussion section, we present the characterization of the Si nanocrystals using transmission electron nicroscopy (TEM), X-ray diffraction (XRD), and PL measurements, including the PL data obtained after different storage times of the particles in air. Then, we present the SXF results, which provide direct evidence for the increase of the Si/SiO_2 ratio in the nanoparticles that were exposed to air for one year. Finally, we use the PY-NEXAFS results to estimate the shift in the bandgap induced by shrinking the size of the Si core. We conclude this paper with a summary of the results and their implications to the mechanism of the PL from Si nanocrystals.

EXPERIMENTAL

The Si nanoparticles were prepared by the LVCC method which has been described in several publications [9, 20]. The method is based on coupling laser vaporization of semiconductors or metals with controlled condensation from the vapor phase which eliminates the need for high temperatures and chemical precursors and leads to good control over particles' size and aggregate state. The Si vapor was generated by pulsed laser vaporization using the second harmonic (532 nm) of a Nd:YAG laser (15–30 mJ/pulse). The Si target, with a stated purity of 99.99%, was obtained from Dow Corning. The chamber was filled with He (99.999%) at a pressure of 900 torr. The temperature of the bottom plate was kept at room temperature while the temperature of the top plate, where the nanoparticles were deposited, was kept between –80 °C and –90 °C.

The photoluminescence measurements were performed using third and fourth harmonics of a Nd:YAG laser (355 and 266 nm, photon power density ≈7 mW/cm^2). The luminescence was dispersed by a SPEX 1 m spectrometer equipped with an EMI 9558 photomultiplier (S20 photocathode). WG295 and WG380 filters were used to block the laser light. For dispersed luminescence spectra the photomultiplier output was processed by a PAR Model 162 boxcar averager and recorded by a computer. Time-resolved decays were averaged using a LeCroy 9350 oscilloscope.

The SXF and PY-NEXAFS measurements were performed at the Advanced Light Source on Beamline 8.0.1, which was described in detail elsewhere [19,21]. Emitted radiation was measured with a Rowland circle-type spectrometer utilizing large spherical gratings and a photon-counting area detector. Total instrumental resolution in the Si *L*-emission region was ~100 meV. The bandwidth of the incident photons used was approximately 50 meV. PY-NEXAFS spectra were acquired by measuring the total Si *L*-emission yield with the same detector used for fluorescence.

RESULTS AND DISCUSSION

Characterization of the Si nanocrystals

Figure 1 displays the XRD pattern of the Si nanocrystals. The spectrum conclusively shows crystalline Si lines 111, 220, and 311 at scattering angles (2θ) of 28, 47, and 56, respectively. Such crystalline lines are not present in the XRD pattern of silica nanoparticles prepared in the presence of O_2 which exhibit a completely amorphous structure similar to that of fumed silica [22].

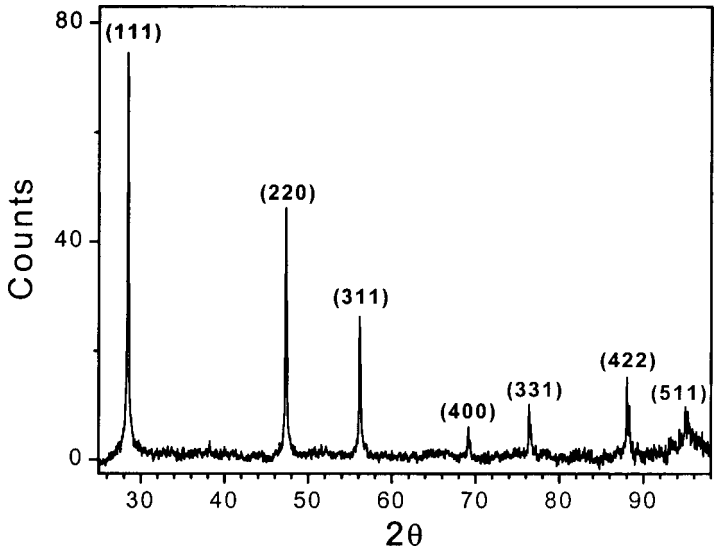

Fig. 1 XRD diffraction pattern of the surface-oxidized Si nanocrystals.

The size and shape of the individual particles were investigated by TEM as shown in Fig. 2a. The Si nanoparticles were found to be spherical with an average diameter of 5–6 nm. Figure 2b shows the electron diffraction pattern of the nanoparticles, which results in d-spacing values, shown in Table 1, in excellent agreement with the corresponding values for bulk silicon crystals.

Table 1 d-spacing calculated from electron diffraction of silicon nanocrystals

d-spacing calculated from electron diffraction of the Si nanocrystals, A°	d-spacing in bulk Si, A°	(hkl) assignments
3.16	3.13	(111)
1.88	1.92	(220)
1.63	1.63	(311)
1.29	1.35	(400)
1.24	1.24	(331)
1.10	1.11	(422)

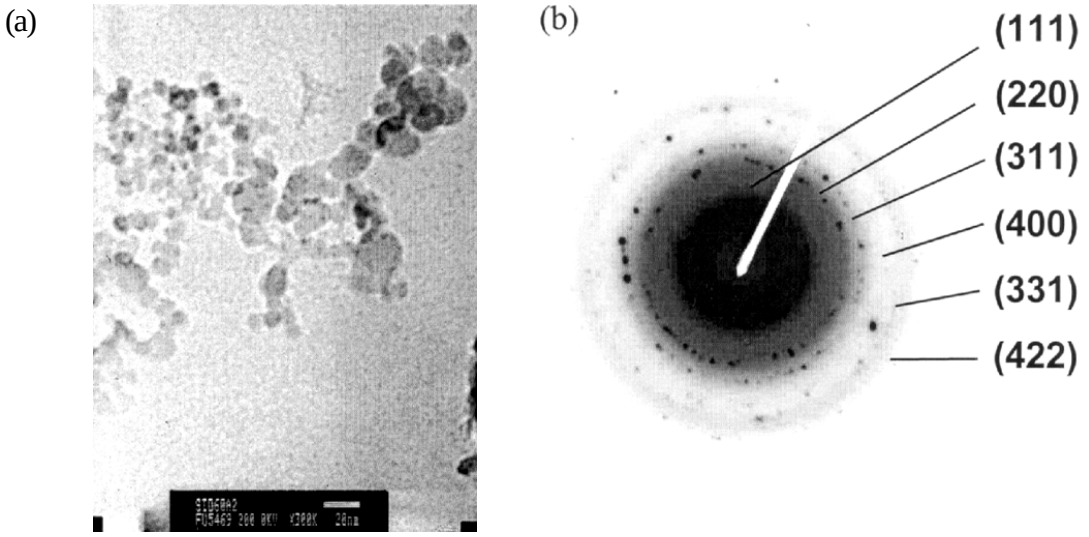

Fig. 2 (a) TEM image and (b) electron diffraction pattern of the Si nanocrystals.

PL of the Si nanocrystals

Dispersed luminescence spectra obtained with 266-nm pulsed laser excitations are shown in Fig. 3. The particles were stored in air for several weeks before the PL measurements.

The spectra differ by the position of the boxcar gate, which ranges from 0 delay with respect to the laser excitation pulse to 25 μs delay. The short delay spectrum enhances the blue emission component, since the lifetime associated with it is short (less than 10 ns) compared to the lifetimes of the red

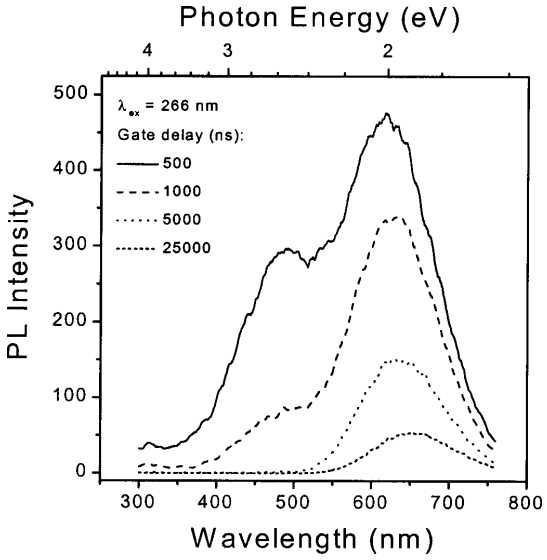

Fig. 3 Dispersed emission of the Si nanocrystals obtained with 266-nm pulsed laser excitation at different gate delays with respect to the excitation pulse.

emission. The shape of the blue emission appears similar to that from SiO_2 nanoparticles, and it is probably due to the oxidized surface layer of the Si nanoparticles [22].

The PL decays of this red emission are multiexponential, and the lifetimes of the photoluminescence are emission wavelength dependent, increasing from short emission wavelength to long emission wavelength. We fit the PL decays with the stretch exponential model [23]:

$$I(t) = I_0 \left(\frac{\tau}{t}\right)^{1-\beta} \exp\left(-\left(\frac{t}{\tau}\right)^{\beta}\right) \tag{1}$$

This decay law is characteristic for systems in which the emitting centers with the decay time τ experience quenching associated with random walks in the fractal space. The scaling factor β is used to approximate the kinetics of the process [23]. We have found that this function gives good fits to the experimental data across the entire spectral range.

It should be noted that completely oxidized Si nanoparticles do not show the red PL observed from the surface-oxidized Si nanocrystals. Rapid oxidation in air can also be induced by the laser excitation. This process is more efficient in freshly prepared nanocrystals before the full development of the surface oxide layer. This is illustrated in Fig. 4, which displays the PL spectra from a freshly prepared Si nanocrystal before and after the irradiation with the 266-nm laser beam (average power ≈55 mW/cm^2). The disappearance of the red emission characteristic of Si nanocrystal core and the appearance of the blue emission characteristic of the silicon oxide nanoparticles are clearly evident in Fig. 4. The sample color also changes from dark yellow into white after the laser oxidation process.

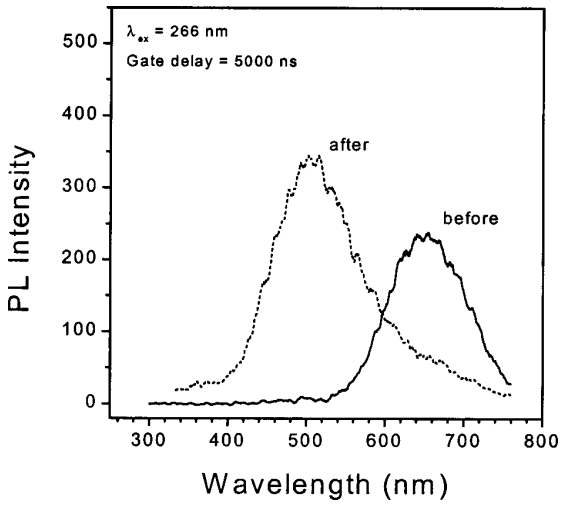

Fig. 4 PL from freshly prepared Si nanoparticles before and after the 266-nm laser irradiation.

The comparison of the PL from Si nanoparticle samples stored in air for different times provides evidence for the slow oxidation of the Si core in air. Figure 5 compares the PL from two samples that were stored in air for 12 and 28 months. A significant blue-shift in the red PL peak is observed in the older sample. The measured lifetimes also decrease in the older sample, which is consistent with decreasing the size of the Si core crystallites.

In order to follow the gradual shift of the red PL peak, we examined three new samples of Si nanocrystals prepared under identical conditions. The PL spectra from the three samples were mea-

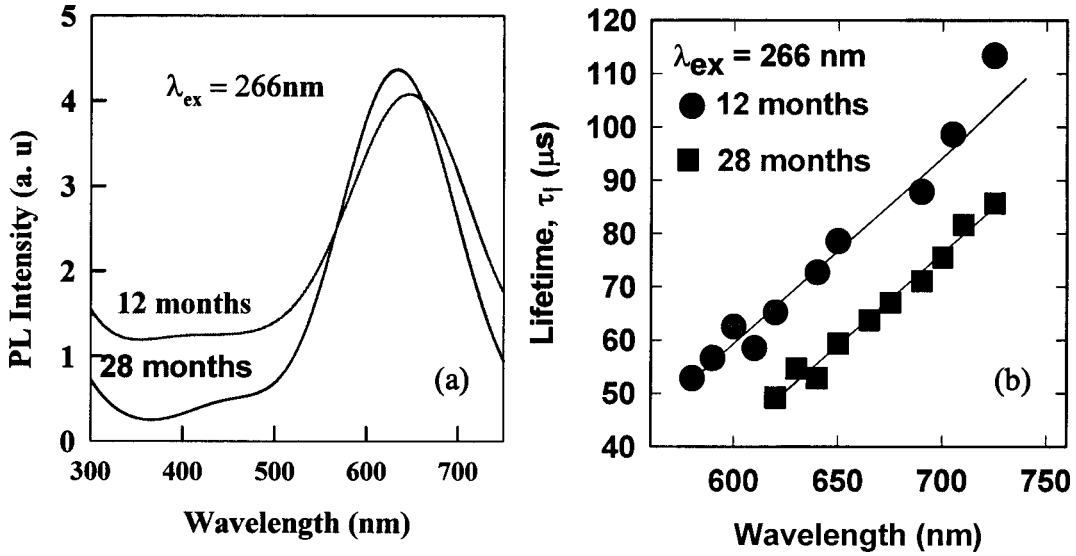

Fig. 5 (a) Comparison of PL from 12-month- and 28-month-old Si nanoparticle samples. (b) Comparison of decay curves from 12-month- and 28- month-old samples.

sured after exposing the particles to ambient air for different time intervals. As shown in Fig. 6, a systematic blue-shift is observed as the exposure time of the particles in air increases. This result confirms the trend observed and strongly suggests that the size of the Si core decreases as further slow oxidation of the particles in air takes place.

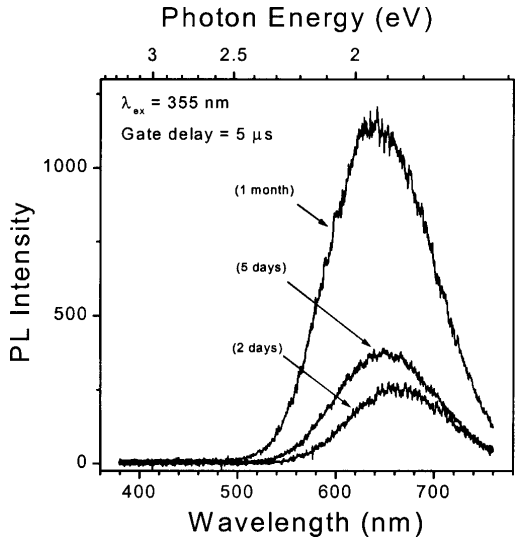

Fig. 6 PL from three samples after different exposure times in air.

SXF and NEXAFS Results

In the present study results from three different types of samples, as well as data from a crystalline silicon reference sample (c-Si), will be discussed. Data acquired from freshly made n-Si nanocrystals will be denoted "n-Si_{new}", whereas nanocrystals synthesized under identical conditions that were allowed

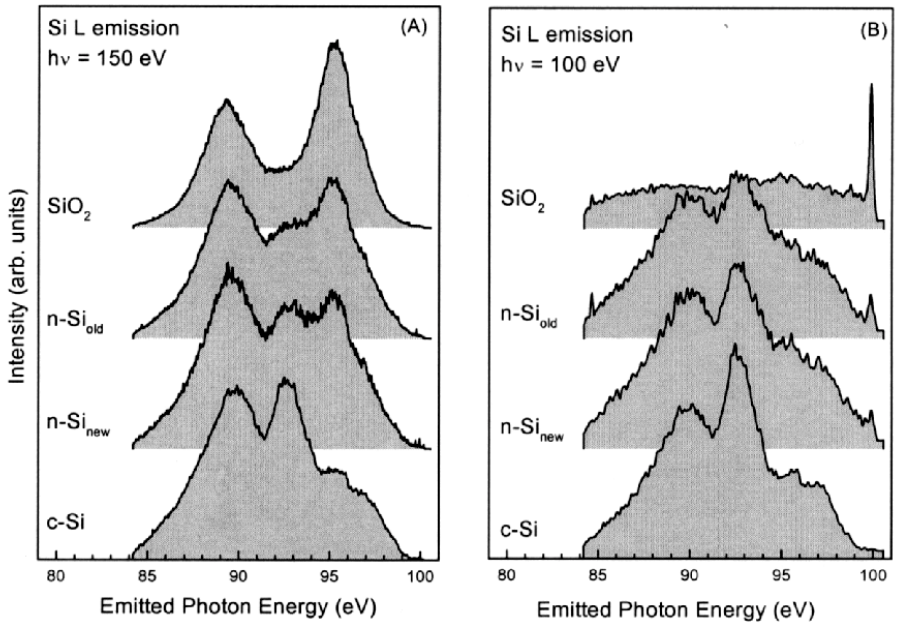

Fig. 7 Si *L*-emission spectra obtained from a cubic silicon reference (c-Si), an SiO_2 reference, Si nanoclusters that were one week old (n-Si_{new}), and nanoclusters that were allowed to age in air for one year (n-Si_{old}). The data shown in (A) were acquired using 150 eV photon energy, whereas the data shown in (B) were obtained using 100 eV photon energy. The data obtained using 150 eV photons shows that the clusters consist of a combination of pure Si and oxidized Si, and that the relative proportion of the two changes slowly over the period of one year. The data in the right pane shows that the pure Si that exists in the core of the nanoclusters is crystalline, not amorphous.

to sit in air for one year will be denoted "n-Si_{old}". Results from silicon oxide nanoparticles made in a high oxygen content environment will be denoted "n-SiO_2".

Data that summarizes the occupied-state SXF measurements acquired from all the samples considered are shown in Fig. 7. Figure 7a shows data taken using an excitation energy of 150 eV, whereas the data in Fig. 7b was obtained using hν = 100 eV. Variation of the excitation energy allows for the emission by pure Si to be isolated from emission from Si in SiO_2. This is due to the difference in the Si 2p binding energy in bulk Si (99.4 eV) compared to SiO_2 (103.6) eV. A detailed comparison of these two data sets allows for the relative amounts of pure Si versus SiO_2 to be readily determined, and also whether the relative proportions of these two species change as the particles oxidize in air.

At the bottom of Figs. 7a and 7b are results obtained from the cubic-Si reference. The major features arise from the *sp*-bands in Si, which give rise to the peaks at 90 and 93 eV in the Si *L*-emission spectrum. It is important to note that similar emission spectra from amorphous Si do not show two separate emission features at 90 and 93 eV, but rather a continuous band of emission centered at ~91 eV [24]. Since the Si 2p core-level binding energy is ~99.6 eV [25], we should expect the two spectra obtained at different photon energies to be essentially the same, and this is what is largely observed.

The uppermost spectra in Figs. 7a and 7b were obtained from the n-SiO_2 nanoclusters, which are expected to consist of essentially pure SiO_2 with no suboxides. Note that the lack of emission from these samples in Fig. 7b confirms this. The two prominent emission features located at 96 and 89 eV arise due to silicon–oxygen bonding. This spectrum is essentially identical to previous ones obtained from glass [26].

The remaining spectra in Figs. 7a and 7b are the chief focus of this work. Upon inspection of these data, several straightforward observations can be made. First, it is immediately obvious that the emission from the n-Si_{new} and n-Si_{old} nanocrystals are nearly similar, and that both are apparently a combination of emission from pure Si (note the feature at 93 eV in both of these spectra) and SiO_2. In fact, a simple linear combination of the two reference spectra reproduces all of the emission features observed in the data from each of the oxidized nanocrystals. Second, based on a least-squares fit, the relative proportion of Si to SiO_2 is 5/4 in the n-Si_{new} nanoparticles and 1/2 in the n-Si_{old} particles. Clearly, as the nanoclusters are exposed to air for one year, a significant decrease in the Si-to-SiO_2 ratio is observed. However, their bonding structure does not change in a dramatic way. Whether the pure Si present is crystalline or amorphous is answered readily in Fig. 7b. Clearly, the Si *L*-emission acquired below using hν = 100 eV from both the new and old nanocrystals exhibit the same emission features at 90 and 93 eV, is observed from the cubic-Si reference. The signal-to-noise ratio in the data from the older nanoparticles is weaker compared to the new, which indicates once again that the component of the nanoparticles that is pure Si is being slowly consumed as they are exposed to air.

The amount of suboxides present in the samples is addressed in Fig. 8. Figures 8a and 8b show Si *L*-emission data taken using different excitation energies from the n-Si_{new} and n-Si_{old} nanoparticles,

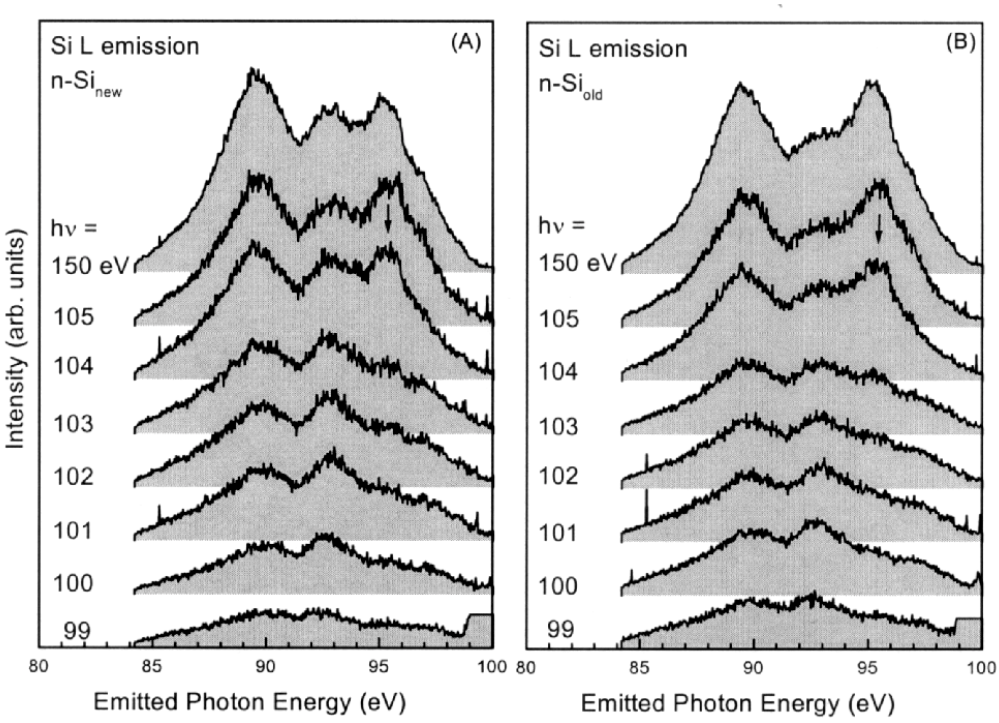

Fig. 8 SXF emission spectra taken using multiple excitation energies, from the new (A) and old (B) n-Si samples. Variation of the excitation energy used allows for the relative amounts of suboxides present in the nanoparticles to be determined. In both sets of data, the lack of change in the emission for excitation energies between 99.0 and 103.0 eV indicates that very few suboxides are present in these particles. The fact that this holds true for the older particles further indicates that no new suboxides are created as the nanoparticles slowly oxidize over the period of 1 year. The arrow indicates the emission from SiO_2, which first appears using a incident photon energy of 104.0 eV.

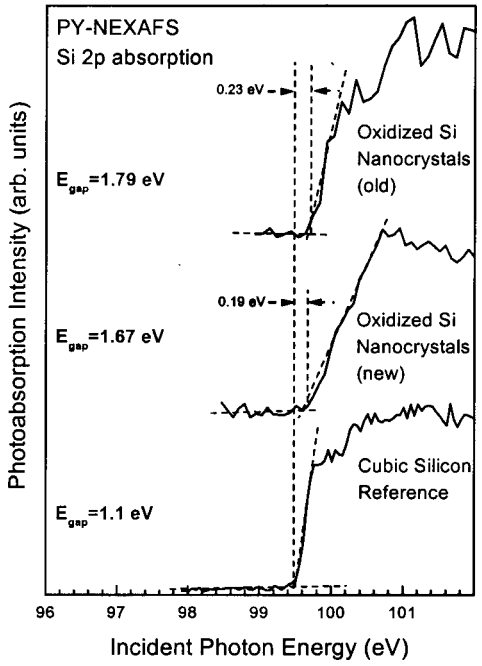

Fig. 9 Photon-yield NEXAFS data obtained from the new and old oxidized silicon nanocrystals and from the c-Si reference. Compared to the reference sample, the absorption threshold is observed to be shifted in the nanocrystals relative to the bulk, and the magnitude of the shift in the older nanocrystals is greater than for the fresh ones.

respectively. The excitation energies used cover the range of Si 2p core-level binding energies for silicon in different oxidation states, from pure silicon (Si^{0+} at 99.6 eV) through SiO_2 (Si^{4+} at 103.6 eV). If significant amounts of suboxides were present in these systems, then the emission spectra would change as the excitation energy gradually increases in Figs. 8a and 8b. Instead, the spectra obtained using excitation energies from 99.0 to 103.0 eV are observed to have the same line shape. Only when the photon energy reaches 104.0 eV does the onset of oxide emission appear (see arrows in Figs. 8a and 8b). This indicates that very few suboxides are present in these oxidized nanoparticles. Furthermore, no new suboxides are created as the particles age over the 1-year time period.

Combining the data in Figs. 7 and 8 with the TEM-based size distribution data discussed above, we now construct the following picture of the morphology of the nanoparticles: They consist of a pure crystalline Si core surrounded by nearly pure SiO_2 shell. Based on the TEM and SEM results that indicate that the mean size of the nanoclusters is about 7.0 ± 0.5 nm, and the changes in the relative proportions of the two types of Si present, that the radius of the inner core of pure crystalline silicon changes from 5.0 ± 0.5 nm to 4.0 ± 0.5 nm over the course of one year.

The variation in the width of the fundamental gap as the nanoparticles oxidize is now addressed by using photon-yield NEXAFS, which gives complementary information on the density of unoccupied states within the particles. These results are summarized in Fig. 9. Compared with the observed position of the Si 2p absorption edge in the cubic-Si reference, we find this edge shifts by ΔE_{CB} = 0.19 eV and 0.23 eV in the new and old nanoparticles, respectively. Since the valence band edge moves by an amount equal to twice this shift [27], we may calculate the change in the gap by using the relation

$$E_{gap} = 3 \cdot \Delta E_{CB} + E_{gap}^{Si} \tag{2}$$

where E_{gap}^{Si} = 1.1 eV is the size of the fundamental gap in pure silicon. Using eq. (2) above, we determine that the bandgap in the new-Si nanoparticles is 1.67 ± 0.05 eV, and that the gap changes to 1.79 ± 0.05 eV as the nanoparticles oxidize.

Based on the analysis of the morphology of the nanoclusters, we conclude that the change in size of the bandgap of the pure Si core is a consequence of the reduction in the physical size of the core. Our measured variation is in good agreement with other works. These include the study of Si nanoparticles using photoemission and electron-yield NEXAFS by Van Buuren et al. [28], the PL data from Schuppler et al. [29], the theoretical results from Wang and Zanger [30] and from Trwoga et al. [31].

CONCLUSIONS

Based on this work, we conclude the following: (1) Freshly prepared Si nanoparticles are composed of a pure, crystalline Si core incased within a nearly pure SiO_2 shell. Very few suboxides are present. (2) As the surface-oxidized Si nanoparticles age in air, the relative proportions of Si and SiO_2 change. However, no new suboxides are formed during this process. (3) The change in the bandgap as a result of shrinking the size of the Si core is directly responsible for the blue-shift observed in the PL data over time.

ACKNOWLEDGMENTS

We would like to thank T.A. Callcott (Tennessee) and Dr. D. L. Ederer (Tulane) for the use of their Soft-X-ray spectrometer on BL 8.0.1 at the Advanced Light Source. The authors gratefully acknowledge financial support from the NASA Microgravity Materials Science Program (Grant NAG8-1484). This research was also supported by the Research Corporation and the National Science Foundation. The Advanced Light Source is supported by the Office of Basic Energy Sciences, Department of Energy.

REFERENCES

1. L. T. Canham. *Appl. Phys. Lett.* **57**, 1046, (1990).
2. W. L. Wilson, P. F. Szajowski, L. E. Brus. *Science* **262**, 1242, (1993).
3. L. J. Brus. *Phys. Chem.* **98**, 3575, (1994).
4. Y. Kanemitsu. *Phys. Rev. B* **49**, 16845, (1995).
5. Y. Kanemitsu. *Phys. Rep.* **263**, 1–91, (1995).
6. L. Brus, P. F. Szajowski, W. L. Wilson, T. D. Harris, S. Schuppler, P. H. Citrin. *J. Am. Chem. Soc.* **117**, 2915, (1995).
7. S. M. Prokes. In *Nanomaterials: Synthesis, Properties and Applications*, A. S. Edelstein, R. C. Cammarata (eds.), Chap. 17, pp. 439–457, Institute of Physics Publishing, Bristol and Philadelphia (1996).
8. T. P. Sidiki, C. M. Sotomayor-Torres. In *Handbook of Nanstructured Materials and Nanotechnology,* H. S. Nalwa (ed.), Vol. 3, pp. 233–289, Academic Press (2000).
9. S. Li, S. J. Silvers, M. S. El-Shall. *J. Phys. Chem.* **101**, 1794, (1997).
10. S. Li and M. S. El-Shall. *Appl. Surf. Sci.* **127**, 330–338 (1998).
11. S. Li, I. N. Germanenko, M. S. El-Shall. *J. Phys. Chem.* **102**, 7319–7322 (1998).
12. N. Hill and K. Whaley. *Phys. Rev. Lett.* **75**, 1130, (1995).
13. C. Delerue, G. Allan, M. Lannoo. *Phys. Rev. B* **48**, 11024, (1993).
14. L. Wang and A. J. Zunger. *Phys. Chem.* **98**, 2158, (1994).
15. T. Takagahara and K. Takeda. *Phys. Rev. B* **46**, 15578, (1993).
16. J. Proot, C. Delerue, G. Allan. *Appl. Phys. Lett.* **61**, 1948, (1992).
17. F. Koch, V. Petrova-Koch, T. Muschik, A. Nikolov, V. Gavrilenko. *Mater. Res. Soc. Symp. Proc.* **283**, 197, (1993).

18. P. Fauchet. *Mater. Res. Soc. Symp. Proc*. **298**, 271, (1993).
19. J. E. Nordgren. *J. Electron Spect. Rel. Phen.* **78** 25 (1996); J. E. Nordgren, *Physica Scripta* **T61**, 32 (1996); D. L. Ederer, T. A. Callcott, R. C. C. Perera. *Synchrotron Radiation News* **7**, 29 (1994). More information about the ALS can be found at http://www-als.lbl.gov/.
20. M. S. El-Shall and S. Li. In *Advances in Metal and Semiconductor Clusters*, M. A. Duncan (ed.), pp. 115–177, JAI Press, London (1998).
21. Beamline 8.0.1 is described further in J. J. Jia, T. A. Callcott, J. Yurkas, A. W. Ellis, F. J. Himpsel, M. G. Samant, J. Stöhr, D. L. Ederer, J. A. Carlisle, E. A. Hudson, L. J. Terminello, D. K. Shuh, R. C. C. Perera. *Rev. Sci. Instrum.* **66**, 1394 (1995); See also http://saturn.vcu.edu/~jacarlis/BL8.htm
22. M. S. El-Shall, S. Li, T. Turkki, D. Graiver, U. C. Pernisz, M. E. Baraton. *J. Phys. Chem*. **99,** 17805 (1995).
23. S. V. Gaponenko, E. P. Petrov, U. Woggon, O. Wind, C. Klingshirn, Y. H. Xie, I. N. Germanenko, A. P. Stupak. *J. Luminescence* **70**, 346, (1996).
24. J. A. Carlisle, A. Chaiken, R. P. Michel, L. J. Terminello, T. A. Callcott, J. J. Jia, D. L. Ederer. *Phys. Rev.* B **53**, R8824 (1996).
25. J. A. Carlisle, M. T. Sieger, T. Miller, T.-C. Chiang. *Phys. Rev. Lett.* **71**, 2955 (1993).
26. T. A. Callcott, (private communication).
27. S. Y. Ren and J. D. Dow. *Phys. Rev.* B **45**, 6492 (1992).
28. T. van Buuren, L. N. Dinh, L. L. Chase, W. J. Siekhaus, L. J. Terminello. *Phys. Rev. Lett.* **80**, 3803 (1998).
29. S. Schuppler, S. L. Friedman, M. A. Marcus, D. L. Adler, Y. H. Xie, F. M. Ross, Y. J. Chabal, T. D. Harris, W. L. Brown, E. E. Chaban, P. F. Szajowski, S. B. Christman, P. H. Citrin. *Phys. Rev. B* **52**, 4910 (1995).
30. L. Wang and A. Zunger. *Phys. Chem.* **98**, 2158 (1994).
31. P. F. Trwoga, A. J. Kenyon, C. W. Pitt. *J. Appl. Phys.* **83**, 3789 (1998).